

Route from spontaneous decay to complex multimode dynamics in cavity QED

Dmitry O. Krimer, Matthias Liertzer, and Stefan Rotter

Institute for Theoretical Physics, Vienna University of Technology, A-1040 Vienna, Austria

Hakan E. Türeci

Department of Electrical Engineering, Princeton University, Princeton, New Jersey 08544, USA

(Received 17 June 2013; published 11 March 2014)

We study the non-Markovian quantum dynamics of an emitter inside an open multimode cavity, focusing on the case where the emitter is resonant with high-frequency cavity modes. Based on a Green's-function technique suited for open photonic structures, we study the crossovers between three distinct regimes as the coupling strength is gradually increased: (i) overdamped decay with a time scale given by the Purcell modified decay rate, (ii) underdamped oscillations with a time scale given by the effective vacuum Rabi frequency, and (iii) pulsed revivals. The final multimode strong-coupling regime (iii) gives rise to quantum revivals of the atomic inversion on a time scale associated with the cavity round-trip time. We show that the crucial parameter to capture the crossovers between these regimes is the nonlinear Lamb shift, accounted for exactly in our formalism.

DOI: [10.1103/PhysRevA.89.033820](https://doi.org/10.1103/PhysRevA.89.033820)

PACS number(s): 42.50.Pq, 42.50.Ar, 42.50.Ct

I. INTRODUCTION

Controlling the emission properties of quantum systems is at the heart of a number of fields ranging from quantum information processing to single-molecule spectroscopy. In solid-state cavity QED a substantial amount of experimental effort aims at designing highly structured photonic environments in the vicinity of the emitter to achieve a high level of control over its quantum dynamics [1–4]. Much of the earlier work focuses on the resonant coupling to a single confined mode of the photonic structure that has favorable emission properties, while coupling to the rest of the modes of the photonic environment is regarded as a parasitic influence and is either discarded or bulked into a total background spontaneous emission rate in the spirit of Ref. [5]. Recent trends in experimental work, however, point towards spatially highly complex and open photonic structures, where the delineation between a cavity and the radiative environment becomes highly blurred (see, e.g., [6–8]). Such situations are more effectively described through the local density of photonic states (LDOPS) [9–15]. This more powerful and potent theoretical approach has meanwhile fueled a great deal of research on light-matter interaction in fields ranging from cavity QED to photovoltaics [16], giving rise to what may be referred to as LDOPS engineering.

While recent theoretical works have recognized the potential of this method [11–13,17], including those dealing with dispersing and absorbing media [9,18], the lack of a suitable method that allows tackling the often complex non-Markovian dynamics of a two-level-like emitter in a leaky photonic structure was a significant hurdle in revealing novel phenomena that may be at play in a host of modern-day light-confining structures such as periodic [2], deterministic aperiodic [19], and disordered photonic media [6], as well as nanoplasmonic systems [20]. Here we present a formalism for computing the full quantum dynamics of emitters in arbitrarily complex photonic structures based on a single Volterra equation with a spectral function proportional to the LDOPS. We then illustrate the possibility of calculating the LDOPS of open and complex photonic structures employing the non-Hermitian set of constant-flux (CF) states that have been introduced

in Ref. [21] to describe steady-state lasing characteristics of lasers. Based on this powerful tool, we explore the dynamics of a quantum emitter in the multimode regime, i.e., when the emitter couples to several modes of the cavity. This regime is notoriously difficult because it leads to highly complex non-Markovian dynamics, but it best illustrates the potency of the method outlined here to provide insight into the various possible time scales of the emitter dynamics. In particular, we discuss a series of crossovers between three dynamical regimes as the coupling strength of the emitter is increased. Some of the aspects of these regimes have been discussed before in the literature within the limited scope of a variety of methods [9,22–27]. The beauty of our approach that we present here is that it provides a unified description, a thorough understanding, and a classification for all of these regimes, with a key parameter being the nonlinear Lamb shift.

II. THEORETICAL MODEL

The system we study is a typical cavity QED setup consisting of a two-level system (TLS) with transition frequency ω_a placed inside a cavity. The method we present here is valid for an arbitrarily complex open cavity geometry, but for the sake of transparency we discuss here a Fabry-Pérot cavity formed by two highly reflecting mirrors (see Fig. 1). To describe the excitation dynamics of the TLS we start with the familiar Hamiltonian written in terms of the modes-of-the-universe approach [28], which makes no distinction between the cavity and its environment, $\mathcal{H} = (\hbar\omega_a/2)\sigma_z + \int d\omega \hbar\omega a^\dagger(\omega)a(\omega) + \hbar\sqrt{\gamma/\pi} \int d\omega [g(\omega, \mathbf{r})a(\omega)\sigma^+ + g^*(\omega, \mathbf{r})a^\dagger(\omega)\sigma^-]$. Here $a^\dagger(\omega)$ and $a(\omega)$ are standard creation and annihilation operators of a photon and $\sigma^+, \sigma^-, \sigma_z$ are the Pauli operators associated with the TLS. The interaction part of \mathcal{H} is written in the electric dipole and rotating-wave approximation, where $g(\omega, \mathbf{r})$ are the coupling amplitudes, and γ stands for the coupling strength proportional to the dipole moment squared. Due to the rotating-wave approximation, nonresonant terms (proportional to $a_\lambda\sigma^-$ and $a_\lambda^\dagger\sigma^+$) are absent in this Hamiltonian such that the number of excitations is conserved. We can thus make the following ansatz for the time evolution of the system: $|\Psi(t)\rangle =$

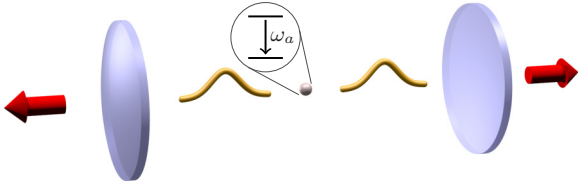


FIG. 1. (Color online) Two-level system with transition frequency ω_a inside an open cavity.

$c(t)e^{-i\omega_a t/2}|u\rangle|0\rangle + \int d\omega c_\omega(t)|l\rangle|1_\omega\rangle e^{-i(\omega-\omega_a/2)t}$, where the ket vectors $|u\rangle$ and $|l\rangle$ stand for the atom in the upper and lower states, respectively, and the ket vectors $|0\rangle$ and $|1_\omega\rangle$ represent the vacuum state and a single photon with the frequency ω . Solving the Schrödinger equation with this ansatz $\mathcal{H}|\Psi(t)\rangle = i\hbar\partial_t|\Psi(t)\rangle$, we arrive at the Volterra equation for the excited-state amplitude of the TLS $c(t)$,

$$\dot{c}(t) = -\frac{\gamma}{\pi} \int_0^t dt' \int_0^\infty d\omega F(\omega) e^{-i(\omega-\omega_a)(t-t')} c(t'), \quad (1)$$

where $F(\omega) = \rho(\mathbf{r}_a, \omega)|g(\omega)|^2$ is the spectral function, featuring the LDOPS $\rho(\mathbf{r}_a, \omega)$, evaluated at the emitter position $\mathbf{r} = \mathbf{r}_a$, and $g(\omega)$ is the frequency-dependent coupling amplitude.

Note that Volterra equations as above have already been used (i) for describing a single discrete energy level coupled to a featureless continuum of states [29] as well as (ii) for the case of a TLS coupled to dispersing dielectrics [9,30]. In the former case (i) a very intuitive graphical analysis was presented including, however, a spurious integral extension towards negative frequencies. In the second case (ii) the solutions were calculated explicitly without, in turn, the insight provided by the modes of the corresponding open cavity geometry. In the following we introduce a method that is general enough to overcome the limitations of both approaches.

To make contact with the physics of an open cavity, we first evaluate the LDOPS for a one-dimensional cavity of length L bounded at $x = 0, L$ by two thin semitransparent mirrors modeled by dielectric slabs of width $d \ll L$ with refractivity index n (see Fig. 1). In what follows we use units where the speed of light $c = 1$. We also normalize x to L and measure time t in units of half the cavity round-trip time and frequency ω in units of its inverse. In

the limit of $n \rightarrow \infty$ and $d \rightarrow 0$ the mirror's transparency is characterized by a factor $\eta = n^2 d$, which is related to the frequency-dependent mirror reflection amplitude as $r(\omega) = i\omega\eta/(2 - i\omega\eta)$ [31]. For such an open system the LDOPS is given exactly by the imaginary part of the Green's function [32] $\rho(x_a, \omega) = -2\omega \text{Im} G^+(x_a, x_a, \omega)/\pi$, where the retarded Green's function (labeled by $+$) satisfies the Helmholtz equation $(\partial_x^2 + n^2\omega^2)G^+(x, x_a, \omega) = -\delta(x - x_a)$ for all $x \in \mathbb{R}$. Note that, due to the openness of the cavity, the LDOPS is a continuous function, corresponding to a continuum of extended modes that are notably different from the discrete set of cavity modes. An exact discrete spectral representation for the Green's function can, however, be obtained for the finite but open cavity geometry at the expense of introducing a non-Hermitian set of modes referred to as CF states, recently introduced to laser physics [21,33]. To compute the response to a monochromatic source at frequency ω , CF states $\phi_m(x)$ have to be determined that satisfy $[\partial_x^2 + n^2\omega_m(\omega)^2]\phi_m(x) = 0$ with the outgoing boundary conditions $\partial_x\phi_m(x) = \pm i\omega\phi_m(x)$ at the right (with $+$) and left cavity boundary (with $-$). These states can be understood to carry a constant flux to infinity [21]. The resulting non-Hermitian eigenvalue problem features complex eigenvalues ω_m and a complete set of right (ϕ_m) and left ($\tilde{\phi}_m$) eigenvectors that parametrically depend on ω and are biorthogonal to each other, $\int_0^L dx n^2 \tilde{\phi}_m^* \phi_n = \delta_{mn}$. The spectral representation of the Green's function can then be constructed through $G^+(x, x', \omega) = -\sum_m \phi_m(x, \omega) \tilde{\phi}_m^*(x', \omega) / [\omega^2 - \omega_m^2(\omega)]$, resulting in a LDOPS in the middle of the cavity that consists of a series of peaks, one for each m . In this picture it becomes intuitively clear that the peaks in the LDOPS, which the TLS couples to, arise when (i) the frequency ω is close to one of the CF frequencies ω_m (see the denominator in the Green's function) and (ii) the CF eigenfunction ϕ_m has a sizable value at the position x_a of the TLS (see the numerator). The function $g(\omega)$ that determines the coupling strength to the emitter is given by $|g(\omega)|^2 = (\pi/2)\omega e^{-(\omega-\omega_a)^2/(2\omega_c^2)}$, where we have introduced a Gaussian cutoff at ω_c . In our simulations we varied the cutoff frequency ω_c in a relatively large frequency interval observing qualitatively similar behavior. In what follows we present results for $\omega_c = 2\omega_a$. Putting all terms together, the spectral function in our example is given by

$$F(\omega) = \frac{2n^2\omega e^{-(\omega-\omega_a)^2}}{(n^2+1)^2 - (n^2-1)^2 \cos(2\omega nd) + 2(n^4-1) \cos(\omega L) \sin^2(\omega nd) + 2n(n^2-1) \sin(\omega L) \sin(2\omega nd)}. \quad (2)$$

III. DYNAMICAL SCENARIOS

We now proceed to solve Eq. (1) for a single excitation, initially stored in the TLS $c(0) = 1$. Applying a Laplace transform (see the Appendix), we derive the expression for the amplitude $c(t)$,

$$c(t) = \frac{\gamma}{\pi} e^{i\omega_a t} \int_0^\infty d\omega U(\omega) e^{-i\omega t}, \quad (3)$$

with the kernel function

$$U(\omega) = \lim_{\varepsilon \rightarrow 0^+} \frac{F(\omega)}{[\omega - \omega_a - \gamma\delta(\omega)]^2 + [\gamma F(\omega) + \varepsilon]^2} \quad (4)$$

and the nonlinear Lamb shift

$$\delta(\omega) = \frac{1}{\pi} \mathcal{P} \int_0^\infty d\tilde{\omega} \frac{F(\tilde{\omega})}{\omega - \tilde{\omega}}, \quad (5)$$

where \mathcal{P} denotes the Cauchy principal value. The dominant frequency components entering the dynamics of $c(t)$ are those that are resonant in the kernel function $U(\omega)$. A necessary condition for such resonances to occur is that the first term in the denominator of $U(\omega)$ vanishes,

$$\frac{\omega_r - \omega_a}{\gamma} = \delta(\omega_r). \quad (6)$$

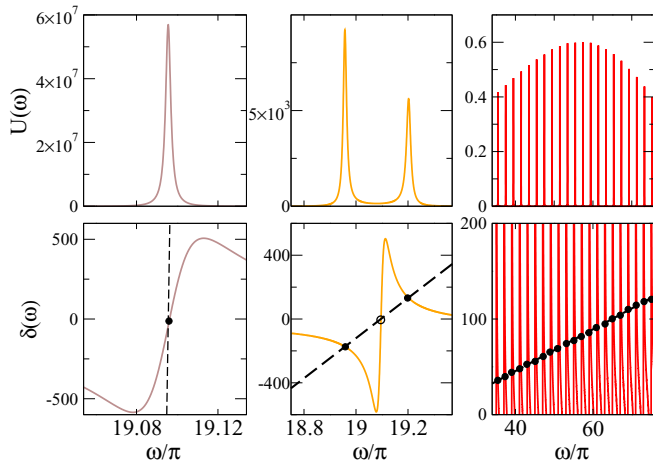


FIG. 2. (Color online) Route from the single-mode to the multi-mode coupling regime for different coupling strengths γ . The top row shows the dimensionless kernel function $U(\omega)$ [Eq. (4)]. The bottom row shows the dimensionless nonlinear Lamb shift $\delta(\omega)$ [Eq. (5)] for the same ω interval as above (note the different zooms for the three columns). The left column shows the weak-coupling regime for $\gamma = 4 \times 10^{-6}$ with a single peak in $U(\omega)$ (Purcell modified spontaneous decay). The middle column shows the strong-coupling regime for $\gamma = 2.5 \times 10^{-3}$ with a well-resolved Rabi splitting in $U(\omega)$ (regime of damped Rabi oscillations). The right column shows the multimode strong-coupling regime for $\gamma = 1.44$ with a multipeak structure in $U(\omega)$ consisting of almost equidistant peaks (regime of revivals). Closed circles label resonance values ω_r of the kernel $U(\omega)$ occurring at the intersections between the Lamb shift $\delta(\omega)$ and the dashed line $(\omega - \omega_a)/\gamma$. At open circles (not shown in right column) such intersections are nonresonant and do not lead to a corresponding peak in $U(\omega)$ (see the text). The transition frequency $\omega_a \approx 19\pi$ of the TLS coincides with the tenth resonance of the spectral function $F(\omega)$ [Eq. (2)]. The reflectivity parameter $\eta = 0.1$ is such that the mirror reflectivity $|r(\omega_a)|^2 = 0.9$. Frequency ω is measured here in units of the inverse half the cavity round-trip time.

This resonance condition is satisfied at the frequencies ω_r , determined by the intersection of the nonlinear Lamb shift $\delta(\omega)$ and a straight line $(\omega - \omega_a)/\gamma$ (see a corresponding graphical analysis in [29] for a simple form of a continuum). Since, according to Eq. (5), every resonance in $F(\omega)$ produces a dip followed by a peak in the Lamb shift, there may be several such intersections, corresponding to multiple solutions of Eq. (6). The corresponding resonances in the kernel $U(\omega)$ can, however, be suppressed, whenever the spectral function $F(\omega)$ has a maximum at the same resonance frequency. This is the case if the kernel $U(\omega) = 1/\gamma^2 F(\omega)$ goes through a minimum at $\omega = \omega_r$.

Based on these observations, we will now investigate the crossover from weak to strong coupling upon variation of the coupling strength γ ; all other parameters, such as the spectral function $F(\omega)$ and the mirror's reflectivity factor η , will be left unchanged. At very weak coupling $\gamma = 10^{-4}$ (left panel of Fig. 2), the straight line in Eq. (6) is very steep and thus leads just to a single intersection, corresponding to a single resonance at $\omega_r \approx \omega_a$. All quantities in Eq. (4) can thus be evaluated at ω_a to very good accuracy and the kernel function reduces to a Lorentzian centered around the slightly shifted

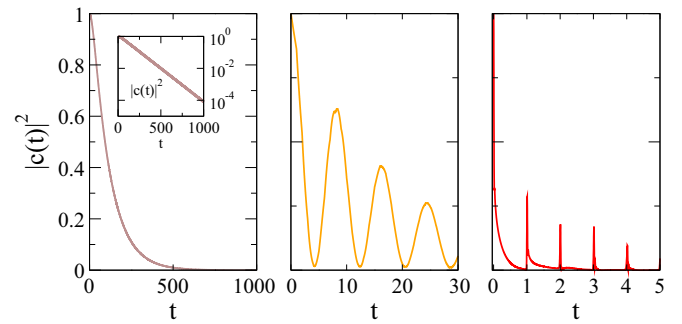


FIG. 3. (Color online) Temporal evolution of the excited-state probability $|c(t)|^2$ of the TLS for the three cases shown in Fig. 2. Time t is measured here in units of half the cavity round-trip time. The left panel shows the weak-coupling regime ($\gamma = 4 \times 10^{-6}$) featuring spontaneous decay (also shown on a log-lin scale in the inset). The middle panel shows the strong-coupling regime ($\gamma = 2.5 \times 10^{-3}$) with damped Rabi oscillations. The right panel shows the multimode strong-coupling regime ($\gamma = 1.44$) featuring pulsed revivals at multiple integers of half the cavity round-trip time.

frequency $\omega_a + \gamma\delta(\omega_a)$ with the width $\gamma F(\omega_a)$. By extending the integration limit in Eq. (3) to $-\infty$, we reproduce the Purcell modified exponential decay of the TLS inversion [23], in good agreement with a numerical solution of the Volterra equation (1) (left panel in Fig. 3). This is the overdamped dynamics of the TLS in the weak-coupling limit of cavity QED.

As γ increases to $\gamma = 2.5 \times 10^{-3}$ we enter the strong-coupling regime, as indicated by the straight line now being flat enough to intersect the nonlinear Lamb shift at three points (middle panel of Fig. 2). Note that these *three* intersections give rise to only *two* resonances ω_r in the kernel $U(\omega)$ since the middle frequency is very close to the resonance of $F(\omega)$ (see the discussion above). As a consequence, the kernel function $U(\omega)$ has a double-peak structure that is characteristic of the single-mode vacuum Rabi splitting [24]. This energy splitting introduces a new frequency scale, the Rabi frequency, which is easily estimated from the resonance condition (6) to be $\sqrt{2\omega_a\gamma}$. The inverse of the peak width provides the time scale at which the Rabi oscillations decay, as confirmed by independent numerical solutions of Eq. (1) (middle panel of Fig. 3).

With a further increase of the coupling strength to $\gamma = 1.44$, the straight line starts to intersect neighboring resonances of $\delta(\omega)$, involving an increasing number of cavity modes. Thus, within the multimode strong-coupling regime it is possible to couple to many cavity modes, including those that reside far away from the transition frequency ω_a (right panel of Fig. 2). Note that, similar to the situation above, only every second intersection with the Lamb shift produces a resonance in the kernel $U(\omega)$ that correspondingly takes on a multi-peaked profile. If, as in our case, these peaks also have an equidistant spacing to each other, then the interference between these resonant modes produces a train of pulses in the probability of the excited state $|c(t)|^2$, corresponding to pulsed revivals of the TLS inversion (right panel of Fig. 3). With the revival time being equal to half the cavity round-trip time, the straightforward explanation of this phenomenon is the repetitive emission and subsequent reabsorption of radiation

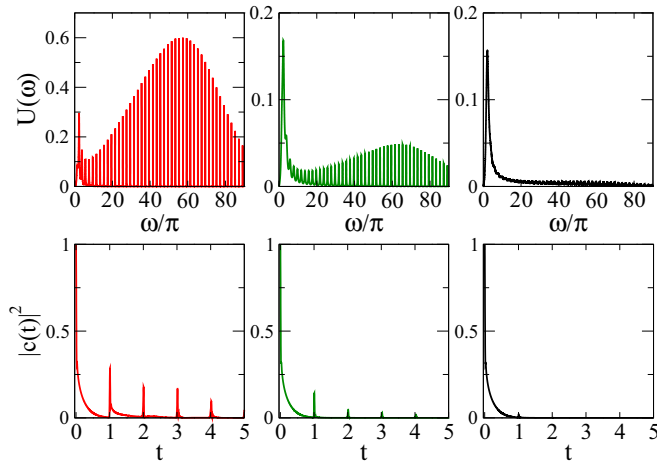


FIG. 4. (Color online) Destruction of the multimode strong-coupling regime by broadening of the peaks in the spectral function (2). The left column shows the mirror reflectivity parameter $\eta = 0.9$ (as in right panel of Fig. 2). The middle column shows $\eta = 0.3$. The right column shows $\eta = 0.015$. The top row shows the dimensionless kernel function $U(\omega)$. The bottom row shows the corresponding excited-state probability $|c(t)|^2$ of the TLS versus normalized time t . The transition frequency $\omega_a \approx 19\pi$ and the coupling strength $\gamma = 1.44$ are the same as in the right panels of Figs. 2 and 3.

by the TLS, when it is back-reflected by the cavity boundaries. As such, this effect relies on the fact that the phases acquired from all possible paths starting from and returning to the position of the TLS differ only by integer multiples of 2π , a condition that strongly depends on the position of the TLS in the cavity. Indeed, if we move the TLS away from the cavity center, a much more irregular type of dynamics emerges (not shown). We also checked explicitly on the limitations that the revival effect is subject to in terms of the cavity opening. For that purpose we performed numerical simulations for cavities with smaller values of the mirror's reflectivity factor $\eta = 0.3, 0.015$ (Fig. 4). We observe that for decreasing values of η the overlap between neighboring resonant peaks in $U(\omega)$ increases until they merge into a single wide resonance. As a result, the revivals in the inversion of the TLS die out when all resonances merge to a single peak, at which point the decay will be just a simple exponential decay, no matter how large the coupling strength γ is.

IV. COMPARISON WITH A SYSTEM-AND-BATH FORMALISM

To verify the validity of the above results, we recalculated the temporal decay in all of the three regimes from above using a recently developed system-and-bath approach [34]. Under the rotating-wave and Born approximations this approach can, in principle, also be reduced to a single Volterra equation as in Eq. (1). We have, however, been able to go beyond the Born approximation by solving a coupled set of Volterra equations for the TLS and damped cavity modes explicitly numerically. These equations very well illustrate how costly it becomes numerically to obtain the solutions for the temporal decay without the Laplace transform employed above and how little

insight one gets into these solutions when they have to be explicitly integrated in time. The fact that we obtain very similar results (for all the scenarios obtained above) with this more complex approach confirms in turn the validity of the simple and insightful strategy presented in the previous sections.

A. Total Hamiltonian

Our starting point is a Hamiltonian that includes altogether five contributions from the resonator, the external region, the TLS and the interaction of the resonator with the external region and of the TLS with the resonator [see Eq. (81) in [34]],

$$\begin{aligned} \mathcal{H} = & \sum_{\lambda} \hbar \omega_{\lambda} a_{\lambda}^{\dagger} a_{\lambda} + \int d\omega \hbar \omega b^{\dagger}(\omega) b(\omega) + \frac{\hbar \omega_a}{2} \sigma_z \\ & + \hbar \sum_{\lambda} \int d\omega [\mathcal{W}_{\lambda}(\omega) a_{\lambda}^{\dagger} b(\omega) + \mathcal{W}_{\lambda}^*(\omega) a_{\lambda} b^{\dagger}(\omega)] \\ & + \sum_{\lambda} [g_{\lambda} a_{\lambda} \sigma^+ + g_{\lambda}^* a_{\lambda}^{\dagger} \sigma^-]. \end{aligned} \quad (7)$$

Note that the form of this Hamiltonian is a bit simpler as compared to the one presented in [34] as we do not consider multiple scattering channels outside the cavity.

The Hermitian resonator modes are described by a discrete set of operators a_{λ} and corresponding eigenfrequencies ω_{λ} , whereas the external radiation field corresponds to a continuous set of operators $b(\omega)$ and frequencies ω . The operators obey the usual canonical commutation relations (see Sec. II D in [34] for more details). The resonator and external region communicate with each other via the coupling matrix elements $\mathcal{W}_{\lambda}(\omega)$ defined as the expectation value of the operator \mathcal{L}_{PQ} sandwiched between the resonator and external modes [see Eq. (52a) in [34]]. This coupling operator is determined through the Feshbach projection formalism, which consists of separating space in two regions, the resonator Q and the external region P . Finally, the action of the operator \mathcal{L} onto an arbitrary function ϕ is written as the decomposition $\mathcal{L}\phi = \mathcal{L}_{QQ}\mu + \mathcal{L}_{QP}\nu + \mathcal{L}_{PQ}\mu + \mathcal{L}_{PP}\nu$, where the functions μ and ν reside inside the resonator and the external regions, respectively. Correspondingly, the operators \mathcal{L}_{QP} and \mathcal{L}_{PQ} act in the vicinity of the boundaries between the resonator and external region (see Secs. II B and III C for more details). The key point is that the total operator \mathcal{L} , the cavity operator \mathcal{L}_{QQ} , and external region operator \mathcal{L}_{PP} are Hermitian operators in their regions of definition. The operators σ_z , σ^+ , and σ^- are the standard Pauli operators that describe the TLS and ω_a stands for its transition frequency. The coupling amplitude g_{λ} is given by

$$g_{\lambda} = -i \left(\frac{\hbar \omega_{\lambda}}{2} \right)^{1/2} \boldsymbol{\mu} \cdot \mathbf{u}_{\lambda}(\mathbf{r}_a), \quad (8)$$

where $\boldsymbol{\mu}$ is the dipole strength of the transition, $\mathbf{u}_{\lambda}(\mathbf{r})$ stands for the eigenfunctions of \mathcal{L}_{QQ} , and \mathbf{r}_a is the location of the TLS.

It should be noted that in the Hamiltonian (7) the rotating-wave approximation has already been applied in the following ways. (i) The nonresonant terms in the system-and-bath part of Hamiltonian [i.e., terms proportional to $a_{\lambda}^{\dagger} b^{\dagger}(\omega)$ and $a_{\lambda} b(\omega)$] are neglected. This approximation is valid if the damping rates

of the cavity resonances are substantially smaller than the frequencies of interest. For our purpose this approximation is indeed well fulfilled since the revival regime that we aim to describe occurs exactly in this limit. (ii) Also the nonresonant terms in the atom-field interaction (i.e., terms proportional to $a_\lambda^\dagger \sigma^+$ and $a_\lambda \sigma^-$) are neglected, which is a commonly used approximation.

B. Volterra equations

Since the Hamiltonian (7) conserves the total number of atom and field excitations (due to the above rotating-wave approximation) we can set up the following ansatz for our solution to the Schrödinger equation:

$$\begin{aligned} |\Psi(t)\rangle = & c(t)e^{-i\omega_a t/2}|u\rangle|0\rangle \\ & + \sum_\lambda c_\lambda(t)|l\rangle|1_\lambda\rangle e^{-i(\omega_\lambda - \omega_a/2)t} \\ & + \int d\omega c(\omega, t) e^{-i(\omega - \omega_a/2)t} |l\rangle|1(\omega)\rangle, \end{aligned} \quad (9)$$

where the ket vectors $|u\rangle$ and $|l\rangle$ stand for the atom in the upper and lower states, respectively. In Eq. (9) the ket vectors $|0\rangle$, $|1_\lambda\rangle$, and $|1(\omega)\rangle$ represent the vacuum state of the electromagnetic field, a single photon in cavity mode λ , and a single photon in the external region with frequency ω , respectively. We assume that the system at time $t = 0$ is in the initial state $|u\rangle|0\rangle$. After straightforward algebra we derive the following set of coupled differential equations for the probability amplitudes $c(t)$, $c_\lambda(t)$, and $c(\omega, t)$ introduced in Eq. (9):

$$\dot{c}(t) = -\frac{i}{\hbar} \sum_\lambda g_\lambda e^{-i(\omega_\lambda - \omega_a)t} c_\lambda(t), \quad (10a)$$

$$\begin{aligned} \dot{c}_\lambda(t) = & -\frac{i}{\hbar} g_\lambda^* e^{i(\omega_\lambda - \omega_a)t} c(t) \\ & - i \int d\omega \mathcal{W}_\lambda(\omega) e^{-i(\omega - \omega_\lambda)t} c(\omega, t), \end{aligned} \quad (10b)$$

$$\dot{c}(\omega, t) = -i \sum_\lambda \mathcal{W}_\lambda^*(\omega) e^{-i(\omega_\lambda - \omega)t} c_\lambda(t). \quad (10c)$$

The initial conditions are $c(0) = 1$ and $c_\lambda(0) = c(\omega, 0) = 0$.

Next, we formally integrate Eq. (10c) and plug the result into Eq. (10b), which allows us to exclude the external region from the consideration such that we finally obtain the set of equations

$$\dot{c}(t) = -\frac{i}{\hbar} \sum_\lambda g_\lambda e^{-i(\omega_\lambda - \omega_a)t} c_\lambda(t), \quad (11a)$$

$$\begin{aligned} \dot{c}_\lambda(t) = & -\frac{i}{\hbar} g_\lambda^* e^{i(\omega_\lambda - \omega_a)t} c(t) - \int d\omega \sum_{\lambda'} \mathcal{W}_\lambda(\omega) \mathcal{W}_{\lambda'}^*(\omega) \\ & \times e^{-i(\omega - \omega_\lambda)t} \int_0^t d\tau e^{-i(\omega'_\lambda - \omega)\tau} c_{\lambda'}(\tau). \end{aligned} \quad (11b)$$

C. Markov approximation

To simplify matters, we apply the so-called Markov approximation in Eq. (11b) with respect to the cavity amplitudes $c_\lambda(t)$ such that memory effects with regard to the

outcoupling to the external radiation field are disregarded. (Note that, most importantly, the memory effects within the cavity are still carried along.) Specifically, we shift the initial time of integration to $-\infty$, let $c_\lambda(t') \approx c_\lambda(t)$, and, assuming subsequent integration with respect to ω , make use of the relation

$$\begin{aligned} e^{-i(\omega - \omega_\lambda)t} \lim_{\sigma \rightarrow 0} \frac{e^{i(\omega - \omega_{\lambda'} - i\sigma)\tau}}{\omega - \omega_{\lambda'} - i\sigma} \Big|_{\tau=-\infty}^{\tau=t} \\ \rightarrow e^{-i(\omega_{\lambda'} - \omega_\lambda)t} \left[\mathcal{P} \left(\frac{1}{\omega - \omega_{\lambda'}} \right) + i\pi \delta(\omega - \omega_{\lambda'}) \right]. \end{aligned} \quad (12)$$

The differential equations for $c(t)$ and $c_\lambda(t)$ are then

$$\dot{c}(t) = -\frac{i}{\hbar} \sum_\lambda g_\lambda e^{-i(\omega_\lambda - \omega_a)t} c_\lambda(t), \quad (13a)$$

$$\begin{aligned} \dot{c}_\lambda(t) = & -\frac{i}{\hbar} g_\lambda^* e^{i(\omega_\lambda - \omega_a)t} c(t) \\ & + \sum_{\lambda'} \Gamma_{\lambda\lambda'}(\omega_{\lambda'}) e^{-i(\omega_{\lambda'} - \omega_\lambda)t} c_{\lambda'}(t), \end{aligned} \quad (13b)$$

where the matrix elements of the damping matrix $\Gamma_{\lambda\lambda'}$ are given by

$$\begin{aligned} \Gamma_{\lambda\lambda'}(\omega_{\lambda'}) = & -\pi \mathcal{W}_\lambda(\omega_{\lambda'}) \mathcal{W}_{\lambda'}^*(\omega_{\lambda'}) \\ & + i\mathcal{P} \int d\omega \frac{\mathcal{W}_\lambda(\omega) \mathcal{W}_{\lambda'}^*(\omega)}{\omega - \omega_{\lambda'}}, \end{aligned} \quad (14)$$

which should be calculated in a discrete set of eigenfrequencies ω_λ only. The second term in Eq. (14) is similar to a Lamb shift in that it accounts for a shift of the cavity resonances in an open system with respect to the positions in the corresponding closed system. Next we formally integrate Eqs. (13a) and (13b) and end up with a set of coupled integral Volterra equations

$$\begin{aligned} c(t) = & 1 - \frac{i}{\hbar^2} \sum_\lambda \frac{g_\lambda g_\lambda^*}{\omega_\lambda - \omega_a} \int_0^t d\tau [e^{-i(\omega_\lambda - \omega_a)(t-\tau)} - 1] c(\tau) \\ & + \frac{1}{\hbar} \sum_{\lambda\lambda'} \frac{g_\lambda \Gamma_{\lambda\lambda'}(\omega'_\lambda)}{\omega_\lambda - \omega_a} \int_0^t d\tau [e^{-i(\omega_\lambda - \omega_a)(t-\tau)} - 1] \\ & \times e^{-i(\omega'_\lambda - \omega_a)\tau} c'_{\lambda'}(\tau), \end{aligned} \quad (15)$$

$$\begin{aligned} c_\lambda(t) = & -\frac{i g_\lambda^*}{\hbar} \int_0^t d\tau e^{i(\omega_\lambda - \omega_a)\tau} c(\tau) \\ & + \sum_{\lambda'} \Gamma_{\lambda\lambda'}(\omega'_\lambda) \int_0^t d\tau e^{-i(\omega_{\lambda'} - \omega_\lambda)\tau} c_{\lambda'}(\tau). \end{aligned} \quad (16)$$

D. One-dimensional dielectric cavity

We solve Eqs. (15) and (16) numerically for the geometry shown in Fig. 1. Specifically, we consider the one-dimensional cavity of length L now bounded at $x = -L, 0$ by two thin semi-transparent mirrors modeled by dielectric slabs of width $d \ll L$ with refractivity index n . Using the fact that the TLS couples only to those modes that are symmetric with respect to the center of the cavity (where the TLS is located), we replace our original geometry by a more simple one. This new cavity runs within $[-L/2, 0^-]$ with Neumann boundary conditions at the position of the TLS $\partial_x u_\lambda(x = -L/2) = 0$. On the right cavity

edge we impose (for the closed system Q) a Dirichlet boundary condition $u_\lambda(x=0^-) = 0$ to remove a singular contribution of the operator \mathcal{L}_{QQ} at this point [see, e.g., Eq. (52a) in [31]]. The corresponding cavity eigenvalue problem

$$\frac{d^2}{dx^2} u_\lambda(x) + \omega_\lambda^2 u_\lambda(x) = 0 \quad (17)$$

is finally solved with the eigenvalues $\omega_\lambda = \pi(2\lambda - 1)/L$ ($\lambda = 1, 2, \dots$) and with the eigenvectors (inside the cavity)

$$u_\lambda = \sqrt{\frac{2}{L}} \cos \left[\omega_\lambda \left(x + \frac{L}{2} \right) \right]. \quad (18)$$

The coupling amplitudes between the TLS and the cavity modes (8) reduce to

$$g_\lambda = i\mu \sqrt{\frac{\hbar\omega_\lambda}{L}} f_c(\omega_\lambda). \quad (19)$$

In the limit of $n \rightarrow \infty$ and $d \rightarrow 0$, keeping the mirror's transparency factor $\eta = n^2 d$ finite, the channel modes (outside the resonator) coincide with those calculated in [31] [see Eqs. (55)–(58) therein],

$$v(\omega, x) = \frac{1}{\sqrt{2\pi}} \left(e^{-i\omega x} + \frac{i - \eta\omega}{i + \eta\omega} e^{i\omega x} \right). \quad (20)$$

To couple these cavity modes in the bounded domain Q to the unbounded domain P we require the coupling elements $\mathcal{W}_\lambda(\omega)$ that enter the damping matrix $\Gamma_{\lambda\lambda'}$,

$$\mathcal{W}_\lambda(\omega) = \frac{(-1)^\lambda}{1 - i\eta\omega} \sqrt{\frac{\omega_\lambda}{\pi\omega L}} f_c(\omega_\lambda). \quad (21)$$

Here and in Eq. (19) we introduce the cutoff function $f_c(\omega_\lambda) = e^{-(\omega_\lambda - \omega_a)^2 / (4\omega_a^2)}$ to eliminate the interaction with high-frequency modes in the same way as was done in Sec. II. To ensure the convergence of the integral in Eq. (14) also in the low-frequency limit, we integrate from a frequency above zero but below the first cavity resonance. Finally, we plug the obtained expressions into Eqs. (14)–(16) and solve them numerically with the initial conditions $c(0) = 1$ and $c_\lambda(0) = 0$.

The results of our calculations are shown in Fig. 5 for two typical values of the coupling strength within both the regime of Rabi oscillations and the regime of revivals. We normalize time to half the cavity round-trip time L/c and find again the revivals occurring at integer multiples of these values. Note in particular the very good correspondence that we find between the results obtained from the model based on the CF state representation of the LDOPS within a single Volterra equation (1) and the system-and-bath formalism given by Eqs. (15) and (16) above. This close correspondence confirms the validity of our calculations and the difference in complexity between the two calculations demonstrates the usefulness of the simple and accessible approach presented in Sec. III.

V. CONCLUSION AND OUTLOOK

To summarize, we have shown how the emission process of a two-level atom changes as a function of its coupling strength to the electromagnetic field of an open multimode resonator. Solving the Volterra equation for the temporal decay through Laplace transform allowed us to obtain the decay

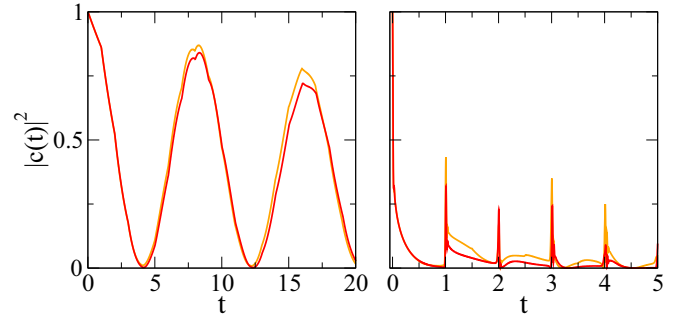


FIG. 5. (Color online) Comparison between the results obtained from a single Volterra equation [dark gray (red) curves] and from the system-and-bath formalism [gray (orange) curves]. The calculations are performed for the 1D geometry presented in Fig. 1 with the mirror reflectivity parameter set to $\eta = 0.18$. The left panel shows $\gamma = 2.5 \times 10^{-3}$ (regime of Rabi oscillations) and the right panel $\gamma = 1.44$ (multimode strong-coupling regime). Time t is measured in units of half the cavity round-trip time.

dynamics together with a corresponding graphical analysis that provides an intuitive understanding of the different regimes observed. On top of the familiar exponential decay and damped Rabi oscillations in the weak- and strong-coupling regimes, respectively, we identify, for very strong coupling, a regime where the emitter couples to multiple modes, leading to pulsed revivals of its initial excitation. We expect that these predictions can be explicitly verified in various physical systems dealing with a two-level-like emitter inside an open multimode cavity. In particular, we have circuit QED setups in mind (e.g., [6,35–37]), for which the coupling strength can be tuned by engineering the two-level system appropriately.

ACKNOWLEDGMENTS

The authors would like to thank R. Luger, M. Malekakhlagh, and C. Viviescas for helpful discussions. Financial support from the Vienna Science and Technology Fund through Project No. MA09-030 (LICOTOLI), the Austrian Science Fund through Projects No. F25-P14 (SFB IR-ON) and No. F49-P10 (SFB NextLite), the National Science Foundation through the NSF CAREER Grant No. DMR-1151810, and the Swiss NSF through Grant No. PP00P2-123519/1 is gratefully acknowledged. We also profited from free access to the computational resources of the Vienna Scientific Cluster.

APPENDIX: LAPLACE TRANSFORM OF THE VOLTERRA EQUATION

We solve the Volterra equation (1) by means of the standard Laplace transform method (see [38,39], where different modal weight functions have been considered), multiplying it by e^{-st} and integrating both sides of the equation with respect to time from 0 to ∞ . Here $s = \sigma + i\omega$ is the complex variable so that we reformulate our problem by solving it in the complex plane of s . After straightforward calculations, the algebraic equation for the Laplace transform $\tilde{c}(s) = \int_0^\infty dt e^{-st} c(t)$ is derived,

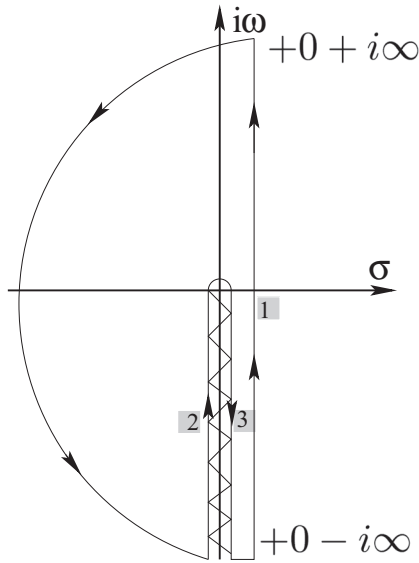


FIG. 6. Contour completion in the complex plane $s = \sigma + i\omega$ for the calculation of the inverse Laplace transform (A2). Those contours that give nonzero contribution are designated by numbers.

which is solved by

$$\tilde{c}(s) = \frac{1}{s + \frac{\gamma}{\pi} \int_0^\infty d\omega \frac{F(\omega)}{s + i(\omega - \omega_a)}}. \quad (\text{A1})$$

Next we perform the inverse Laplace transformation $c(t) = \frac{1}{2\pi i} \int_{\sigma - i\infty}^{\sigma + i\infty} ds e^{st} \tilde{c}(s)$ and obtain the formal solution for the amplitude $c(t)$,

$$c(t) = \frac{e^{i\omega_a t}}{2\pi i} \int_{\sigma - i\infty}^{\sigma + i\infty} \frac{e^{st} ds}{s + i\omega_a + G(s)}, \quad (\text{A2})$$

with

$$G(s) = \frac{\gamma}{\pi} \int_0^\infty \frac{d\omega F(\omega)}{s + i\omega}, \quad (\text{A3})$$

where $\sigma > 0$ should be chosen such that the real parts of all singularities of $\tilde{c}(s)$ are smaller than σ . It can be shown that the function

$$J(\omega) = \lim_{\sigma \rightarrow 0^+} [G(\sigma + i\omega) - G(-\sigma + i\omega)] \quad (\text{A4})$$

is nonzero for $-\infty < \omega \leq 0$. Therefore, the function $G(s)$ and, as a consequence, the whole integrand in Eq. (A2) exhibit a jump along the negative part of the imaginary axis, which is a branch cut. By equating the denominator of Eq. (A2) to zero $s + i\omega_a + G(s) = 0$, the poles s_j are shown to satisfy the equation

$$\omega_j + \omega_a = \frac{\gamma}{\pi} \int_0^\infty d\omega \frac{F(\omega)}{\omega + \omega_j}, \quad \sigma_j = 0. \quad (\text{A5})$$

Thus, the poles (if at all existing) can be located on the imaginary axis only. Moreover, we strictly prove, using a graphical analysis and the fact that $F(\omega) \geq 0$, that only a single simple pole can reside in the positive imaginary axis that leads to undamped oscillations at infinite time. For values of the coupling strength γ larger than considered in this paper, such a scenario emerges in the equations but is not considered here. Thus, to evaluate the original integral (A2), we apply Cauchy's theorem to a closed contour shown in Fig. 6. We prove similarly to Jordan's lemma that the arc contribution is negligible and the contribution of the small semi-circle around $s = 0$ is also zero. Therefore, the only paths that remain are those around the branch cut and the one we are looking for (see Fig. 6). Thus, we derive the following expression for the amplitude $c(t)$:

$$c(t) = \frac{e^{i\omega_a t}}{2\pi i} \int_0^\infty d\omega e^{-i\omega t} [\Phi_-(\omega) - \Phi_+(\omega)], \quad (\text{A6})$$

where

$$\Phi_\pm(\omega) = \lim_{\sigma \rightarrow 0^+} \left\{ \frac{1}{\omega - \omega_a + i \left[\frac{\gamma}{\pi} \int_0^\infty \frac{d\tilde{\omega} F(\tilde{\omega})}{\pm \sigma + i(\tilde{\omega} - \omega)} \pm \sigma \right]} \right\}. \quad (\text{A7})$$

Employing the Sokhotski-Plemelj theorem, the integral in the denominator of Eq. (A7) is rewritten in the limit of $\sigma \rightarrow 0$ as

$$\int_0^\infty \frac{d\tilde{\omega} F(\tilde{\omega})}{\pm \sigma + i(\tilde{\omega} - \omega)} = -i \left\{ \mathcal{P} \int_0^\infty \frac{d\tilde{\omega} F(\tilde{\omega})}{\tilde{\omega} - \omega} \pm i\pi F(\omega) \right\},$$

We finally end up with Eqs. (3)–(5) for the amplitude $c(t)$ (see Sec. III).

-
- [1] G. Khitrova *et al.*, *Nat. Phys.* **2**, 81 (2006).
 [2] S. Noda, M. Fujita, and T. Asano, *Nat. Photon.* **1**, 449 (2007).
 [3] A. Wallraff *et al.*, *Nature (London)* **431**, 162 (2004).
 [4] M. Agio, *Nanoscale* **4**, 692 (2012).
 [5] H. J. Carmichael, R. J. Brecha, M. G. Raizen, H. J. Kimble, and P. R. Rice, *Phys. Rev. A* **40**, 5516 (1989).
 [6] L. Sapienza *et al.*, *Science* **327**, 1352 (2010).
 [7] P. V. Ruijgrok *et al.*, *Opt. Express* **18**, 6360 (2010).
 [8] X.-W. Chen, M. Agio, and V. Sandoghdar, *Phys. Rev. Lett.* **108**, 233001 (2012).
 [9] H. T. Dung, L. Knöll, and D.-G. Welsch, *Phys. Rev. A* **62**, 053804 (2000).
 [10] N. Vats, S. John, and K. Busch, *Phys. Rev. A* **65**, 043808 (2002).
 [11] M. Wubs and A. Lagendijk, *Phys. Rev. E* **65**, 046612 (2002).
 [12] T. Ochiai, J. I. Inoue, and K. Sakoda, *Phys. Rev. A* **74**, 063818 (2006).
 [13] V. S. C. Manga Rao and S. Hughes, *Opt. Lett.* **33**, 1587 (2008).
 [14] R. Pierrat and R. Carminati, *Phys. Rev. A* **81**, 063802 (2010).
 [15] X.-W. Chen, V. Sandoghdar, and M. Agio, *Phys. Rev. Lett.* **110**, 153605 (2013).
 [16] A. Polman and H. A. Atwater, *Nat. Mater.* **11**, 174 (2012).
 [17] P. T. Kristensen, J. Mørk, P. Lodahl, and S. Hughes, *Phys. Rev. B* **83**, 075305 (2011).
 [18] M. Khanbekyan, D.-G. Welsch, C. Di Fidio, and W. Vogel, *Phys. Rev. A* **78**, 013822 (2008); *Phys. Scr.* **T135**, 014015 (2009).

- [19] S. V. Boriskina, A. Gopinath, and L. Dal Negro, *Physica E* **41**, 1102 (2009).
- [20] D. E. Chang, A. S. Sorensen, P. R. Hemmer, and M. D. Lukin, *Phys. Rev. Lett.* **97**, 053002 (2006).
- [21] H. E. Türeci, A. D. Stone, and B. Collier, *Phys. Rev. A* **74**, 043822 (2006).
- [22] V. Weisskopf and E. Wigner, *Z. Phys.* **63**, 54 (1930).
- [23] E. M. Purcell, *Phys. Rev.* **69**, 681 (1946).
- [24] E. T. Jaynes and F. W. Cummings, *Proc. IEEE* **51**, 89 (1963).
- [25] P. W. Milonni, J. R. Ackerhalt, H. W. Galbraith, and M. L. Shih, *Phys. Rev. A* **28**, 32 (1983).
- [26] R. W. F. van der Plank and L. G. Suttorp, *Phys. Rev. A* **54**, 2464 (1996).
- [27] A. Carmele, J. Kabuss, F. Schulze, S. Reitzenstein, and A. Knorr, *Phys. Rev. Lett.* **110**, 013601 (2013).
- [28] R. J. Glauber and M. Lewenstein, *Phys. Rev. A* **43**, 467 (1991).
- [29] C. Cohen-Tannoudji, J. Dupont-Roc, and G. Grynberg, *Atom-Photon Interactions* (Wiley-VCH, Weinheim, 2004), Complement CIII.
- [30] I. V. Bondarev, G. Ya. Slepian, and S. A. Maksimenko, *Phys. Rev. Lett.* **89**, 115504 (2002).
- [31] C. Viviescas and G. Hackenbroich, *J. Opt. B* **6**, 211 (2004).
- [32] E. N. Economou, *Green's Functions in Quantum Physics*, 3rd ed., Springer Series in Solid-State Sciences Vol. 7 (Springer, Berlin, 2006).
- [33] H. E. Türeci, L. Ge, S. Rotter, and A. D. Stone, *Science* **320**, 643 (2008).
- [34] C. Viviescas and G. Hackenbroich, *Phys. Rev. A* **67**, 013805 (2003).
- [35] K. Srinivasan and O. Painter, *Nature (London)* **450**, 862 (2007).
- [36] J. M. Fink *et al.*, *Nature (London)* **454**, 315 (2008).
- [37] A. A. Houck *et al.*, *Phys. Rev. Lett.* **101**, 080502 (2008).
- [38] K. F. Riley, M. P. Hobson, and S. J. Bence, *Mathematical Methods for Physics and Engineering* (Cambridge University Press, Cambridge, 2006).
- [39] P. R. Berman and G. W. Ford, in *Advances in Atomic, Molecular, and Optical Physics*, edited by E. Arimondo, P. R. Berman, and C. C. Lin (Elsevier, Amsterdam, 2010), Vol. 59, Chap. 5, pp. 175–221.